Supplementary Information for

Metastasis of cholangiocarcinoma is promoted by extended high-mannose glycans

Diane Dayoung Park, Chatchai Phoomak, Gege Xu, Laura P. Olney, Khiem A. Tran, Simon S. Park, Nathan E. Haigh, Guillaume Luxardi, Worachart Lert-itthiporn, Michiko Shimoda, Qiongyu Li, Nobuyuki Matoba, Fernando Fierro, Sopit Wongkham, Emanual Maverakis, Carlito B. Lebrilla

Email: dpark4@bidmc.harvard.edu

This PDF file includes:

Other supplementary materials for this manuscript include the following:

SI Materials and Methods

Cell culture. Human cholangiocarcinoma cells (KKU-213A, KKU-213B) were obtained from the Japanese Collection of Research Bioresources Cell Bank (JCRB, Osaka, Japan) and highly metastatic cholangiocarcinoma cells (KKU-213AL5, KKU-213BL5) were established and characterized as previously described (1–3). Cholangiocarcinoma cells were grown in Ham's F12 media supplemented with 10% (v/v) fetal bovine serum (FBS), 100 U/mL penicillin, and 100 μg/mL streptomycin. Human ductal carcinoma cells (HCC1954) were obtained from the American Type Culture Collection (ATCC, Manassas, VA) and grown in Roswell Park Memorial Institute (RPMI)-1640 medium supplemented with 10% (v/v) FBS, 100 U/mL penicillin, and 100 μg/mL streptomycin. Human colorectal adenocarcinoma cells (Caco-2) were obtained from ATCC and grown in Eagle's Minimum Essential Medium (EMEM) supplemented with 10% (v/v) FBS, 100 U/mL penicillin, and 100 μg/mL streptomycin. All cells were maintained at 37˚C in a humidified incubator with 5% CO_2.

Cell treatments. The α-mannosidase inhibitor kifunensine (Santa Cruz Biotechnology, Dallas, TX) was introduced to KKU-213A, KKU-213B, HCC1954, and undifferentiated Caco-2 cells to a final concentration of 0, 1, 10, 20, or 30 μg/mL at 37°C. After 72 h, treated cells were washed with PBS and harvested by scraping for LC-MS/MS analysis. The concentration at which the abundances of high-mannose glycans reached a maximum value was selected for subsequent studies. Concanavalin A from *Canavalia ensiformis* (Vector Laboratories, Burlingame, CA) was introduced to KKU-213AL5 and KKU-213BL5 cells to a final concentration of 0, 0.78, 1.56, 3.13, 6.25, 12.5, 25, 50, 100 μg/mL in serum-free media at 37°C for 1 h to evaluate cell aggregation. Treated cells were subsequently washed with PBS and imaged on a Leica DMI3000B microscope (Leica Microsystems, Wetzlar, Germany). The maximum concentration at which cells did not aggregate was selected for subsequent studies. Avaren was dimerized by fusion to the Fc region of human IgG and produced in *Nicotiana benthamiana* as previously described (4, 5). KKU-213AL5 and KKU-213BL5 cells were treated with Avaren-Fc to a final concentration of 6.25 μg/mL at 37°C for 1 h and washed with PBS prior to initiating migration and invasion assays.

Time-lapse microscopy. A total of 20,000 KKU-213A or KKU-213AL5 cells were seeded in 35 mm tissue culture dishes (Corning, Corning, NY) 24 h prior to imaging. Eight fields of view with approximately the same density of cells were selected per dish at the start of the recording. Images were acquired every 5 min for 24 h on a BioStation IM-Q system (Nikon Instruments, Melville, NY). The chamber was maintained at 37˚C and 5% CO_2. Time-lapse videos were compiled to document all images in series over 24 h.

Flow cytometry. KKU-213A, KKU-213AL5, KKU-213B, and KKU-213BL5 were incubated with Fc-block (BD Biosciences, San Jose, CA) on ice for 15 min and stained with Aqua-LIVE/DEAD (Invitrogen, Carlsbad, CA). Cells were then fixed and permeabilized using the transcription factor staining buffer set (Invitrogen), stained with or without (FMO, Fluorescence Minus One) anti-MAN1A1 antibody (Novus Biologicals, Centennial, CO) for 30 min at room temperature, and stained with anti-Rabbit IgG antibody coupled with Alexa555 (Invitrogen). Cells were washed after each step and before being analyzed on a BD Fortessa flow cytometer (BD, Franklin Lakes, NJ). Data were analyzed using FlowJo (Tree Star, Ashland, OR). After gating single cells and live cells, MAN1A1 fluorescence for each cell type was plotted in histograms and compared with the FMO.

Vector construction. A human MAN1A1 expression plasmid was generated by cloning in the hMan1a1 cDNA obtained from Dharmacon (Lafayette, CO) into a pcDNA 3.1 vector obtained from Thermo Fisher Scientific (Waltham, MA). The plasmid carries the neomycin resistance gene along with a multiple cloning site (MCS) upstream of the CMV promoter.

Transfection. KKU-213AL5 cells were transfected for 24 h with 50 ng plasmid DNA in serum-free Dulbecco's Modified Eagle Media (DMEM) (Gibco, Montgomery County, MD) with 5% (v/v) Lipofectamine (Invitrogen). Overexpression was maintained in DMEM supplemented with 10% (v/v) FBS, antimycotic, penicillin/streptomycin, and 1 mg/mL G418 sulfate (Corning) with daily media change. Cells were harvested at 70-80% confluency to ensure maximal *MAN1A1* expression for subsequent studies.

RNA isolation and qRT-PCR analysis. KKU-213A, KKU-213AL5, KKU-213B, and KKU-213BL5 cells were harvested, washed twice with PBS, and resuspended in RNAlater (Life Technologies, Carlsbad, CA). Total RNA were extracted using RNeasy plus mini kit (Qiagen, Germantown, MD) and the quantity and quality of RNA were determined by using a Qubit Fluorometer (Life Technologies) and TapeStation 2200 (Agilent Technologies, Santa Clara, CA) following the manufacturer's protocol. Total RNA were reverse transcribed to cDNA using iScript Reverse Transcription Supermix (Bio-Rad Laboratories, Hercules, CA) following the manufacturer's protocol. Predesigned human glycosylation and extracellular matrix and cytoskeleton PrimePCR plates (Bio-Rad Laboratories) were used for real-time PCR using the CFX96 Touch Real-Time PCR detection system (Bio-Rad Laboratories) and the analysis was performed using CFX Manager 3.1 (Bio-Rad Laboratories). Gene expression was normalized to reference genes and presented as fold changes.

Cell membrane extraction. Cells were harvested by scraping and resuspended in homogenization buffer containing 0.25 M sucrose, 20 mM HEPES-KOH (pH 7.4), and 1:100 protease inhibitor cocktail (EMD Millipore, Burlington, MA). Cell lysis was performed on ice using a probe sonicator (Qsonica, Newtown, CT) operated with five alternating on and off pulses in 5 and 10 s intervals, respectively. Lysates were centrifuged at 2,000 x g for 10 min to remove the nuclear fraction and cellular debris. The supernatant was transferred to high speed tubes (Beckman Coulter, Brea, CA) and centrifuged at 200,000 x g for 45 min at 4°C using an Optima TLX Ultracentrifuge (Beckman Coulter). Pellets were solubilized and centrifuged in series with 0.2 mM sodium carbonate (pH 11) followed by water to remove other non-membrane fractions. The resulting membrane fraction was stored at -20°C until further processing.

Preparation of N-glycans. The total protein concentration in each membrane fraction was measured using an IMPLEN NanoPhotometer P300 (Implen, Westlake Village, CA) according to the manufacturer's protocol and equalized across all fractions. Each fraction was mixed with a final volume of 100 μL of 100 mM ammonium bicarbonate in 5 mM dithiothreitol and heated for 10 s at 100°C to thermally denature the proteins. To cleave N-glycans from membrane proteins, 2 μL of peptide N-glycosidase F (New England Biolabs, Ipswich, MA) were added to the samples and incubated in a microwave reactor (CEM Corporation, Matthews, NC) for 10 min at

20 watts. After addition of 400 µL of chilled ethanol, samples were placed in -80°C for 1.5 h and centrifuged for 20 min at 21,000 x g to precipitate residual deglycosylated proteins. The supernatant containing the released N-glycans was collected and dried. N-Glycans were purified by solid phase extraction using a porous graphitized carbon (PGC) matrix (Grace, Columbia, MD). Eluted fractions were dried *in vacuo*.

N-Glycomic LC-MS/MS analysis. Glycan samples were reconstituted in nanopure water and analyzed using a nano-LC-Chip-QTOF-MS/MS system (6520, Agilent Technologies). Samples were maintained at 6°C and introduced to the MS with a microfluidic chip, which consists of enrichment and analytical columns packed with PGC and a nanoelectrospray tip. A binary gradient was applied at a flow rate of 0.4 µL/min: (A) 3% (v/v) acetonitrile and 0.1% (v/v) formic acid in water and (B) 90% (v/v) acetonitrile in 1% (v/v) formic acid in water. MS spectra were acquired at 1.5 s per spectrum over a mass range of *m/z* 600-2000 in positive ionization mode. Mass inaccuracies were corrected with reference mass *m/z* 1221.991.
Collision-induced dissociation (CID) was performed with nitrogen gas using a series of collision energies ($V_{collision}$) dependent on the *m/z* values of the N-glycans, based on the equation:

$$V_{collision} = \text{slope } (m/z) + \text{offset},$$

where the slope and offset were set at (1.8/100 Da) V and –2.4 V, respectively.

N-Glycomic data analysis. N-Glycan compounds were identified with an in-house retrosynthetic library of all possible glycan compositions according to accurate mass (6). Subtypes including high-mannose, complex and hybrid N-glycans were grouped by knowledge of the mammalian N-glycan biosynthetic pathway. Signals above a signal-to-noise ratio of 5.0 were filtered and deconvoluted using MassHunter Qualitative Analysis B.06.01 (Agilent Technologies). Deconvoluted masses were compared to theoretical masses using a mass tolerance of 20 ppm and a false discovery rate of 0.6%. Abundances were determined by integrating ion counts for observed glycan masses. Relative abundances were determined by normalizing abundances to the summed peak areas of all glycans detected. Statistical evaluation of significant glycan abundance changes was performed using an unpaired, two-tailed Student's *t*-test.

Preparation of N-glycopeptides. Following lysis and membrane extraction, proteins were denatured in 8 M urea at 55°C, reduced with 18 mM dithiothreitol, alkylated with 27 mM iodoacetamide, diluted to 1 M urea with 50 mM ammonium bicarbonate, and incubated with 1 μg trypsin at 37°C overnight. The resulting peptides were concentrated *in vacuo*. Glycopeptides were enriched by solid-phased extraction using iSPE-HILIC cartridges (Nest Group, Southborough, MA) (7, 8). Cartridges were conditioned with acetonitrile and 0.1% (v/v) trifluoroacetic acid in water, followed by 1% (v/v) trifluoroacetic acid and 80% (v/v) acetonitrile in water. Peptides were loaded onto the column, and washed with 1% (v/v) trifluoroacetic acid and 80% (v/v) acetonitrile in water. Enriched products were eluted with 0.1% (v/v) trifluoroacetic acid in water and dried.

N-Glycoproteomic LC-MS/MS analysis. Purified glycopeptides (1 μg) were loaded using 2% (v/v) acetonitrile and 0.1% (v/v) trifluoroacetic acid in water and analyzed using a reverse-phase Michrom Magic C18AQ column (200 μm, 150 mm) coupled with a Q Exactive Plus Orbitrap mass spectrometer through a Proxeon nano-spray source (Thermo Fisher Scientific). A binary gradient was applied at 0.3 μL/min using (A) 0.1% (v/v) formic acid in water and (B) 0.1% (v/v) formic acid in acetonitrile. Per acquisition, the instrument was run in data-dependent mode as follows: spray voltage, 2.0 kV; ion transfer capillary temperature, 250°C; full scan mass range, *m/z* 700-2000; MS automatic gain control, 1 x 10^6; MS maximum injection time, 30 ms; MS/MS automatic gain control, 5 x 10^4; MS/MS maximum injection time, 50 ms; dynamic exclusion, 10 s; precursor resolution, 70,000; product ion resolution, 17,500; precursor ion isolation width of 1.6 *m/z*; stepped collision energy, higher-energy collisional dissociation (HCD), 17, 27, 37.

N-Glycoproteomic data analysis. Raw data were exported using xCalibur 2.0 (Thermo Scientific). Proteins were identified using Byonic 2.7.4 (Protein Metrics, Cupertino, CA) against the reviewed Swiss-Prot human protein database (20,207 entries) with sample-specific parameters as determined from Preview (Protein Metrics): mass tolerances of 5-10 ppm for the precursor and 10-20 ppm for fragment ions; carbamidomethylation of cysteine as a fixed modification; oxidation of methionine, deamidation of asparagine and glutamine, acetylation of the protein N-terminus, N-terminal pyroglutamate formation of glutamine and glutamate, and N-glycosylation of asparagine (in-house human database of 369 entries) as variable modifications;

two missed cleavage sites. Identifications were filtered with a 1% false discovery rate and were accepted if the following conditions were met: |Log Prob|>2; Delta Mod>10; Byonic score>200. Site-specific quantitation was performed using the area under the curve of the extracted ion chromatogram which was normalized to the total protein concentration. Amino acid frequency plots were exported from WebLogo 3 (9). Functional annotation analysis of proteins was performed using PANTHER 14.1 (10).

3D structure prediction. High-mannose glycans were built using Glycam Carbohydrate Builder and minimized energies were computed for all possible conformational isomers (11). Candidate glycoproteins were selected based on the abundance of extended high-mannose glycans from the site-specific glycosylation analysis. Protein Data Bank (PDB) files of candidate proteins (1CX8; 1JV2; 5FN3) were pre-processed and high-mannose glycosylation sites were identified. Solvent accessible surface area (SASA) was calculated by Naccess 2.1.1 (12).

Molecular dynamics (MD) simulations. The structure of dimeric transferrin receptor protein 1 in the bound state were obtained from the PDB (1SUV bioassembly 1; chain A, B). Simulation input files were generated using CHARMM-GUI 3.0 (13). A cubic water box with an edge distance of 10 Å in each axis was placed to solvate the protein and counter ions K^+ and Cl^- were added to neutralize the overall charge. Site N727 in chains A and B was modified with Man 9, αDMan(1→2)αDMan(1→6)[αDMan(1→2)αDMan(1→3)]αDMan(1→6)[αDMan(1→2)αDMan(1→2)αDMan(1→3)]βDMan(1→4)βDGlcNAc(1→4)βDGlcNAc(1→)Asn, or Man 5, αDMan(1→6)[αDMan(1→3)]αDMan(1→6)[αDMan(1→3)]βDMan(1→4)βDGlcNAc(1→4)βDGlcNAc(1→)Asn. All calculations were performed at 303.15 K and 1 bar with GROMACS 2019.2 (14). All input files were prepared under periodic boundary conditions (PBC) and with the particle-mesh Ewald (PME) technique for long-range electrostatic interactions. Grid parameters for fast Fourier transforms (FFTs) were generated automatically. Generated coordinates of the glycosylated protein/water system were used to perform energy minimization in 5000 steps using the steepest descent algorithm. The minimized coordinates were used to gradually equilibrate each system for 100 ps in constant number of particles, volume, and temperature (NVT) conditions. Extreme Science and Engineering Discovery Environment

(XSEDE) Comet was used for additional equilibration in constant number of particles, pressure, and temperature (NPT) conditions (15). Each system was simulated for 250 ns with a time step of 2 fs using the CHARMM36m force field (16). Covalent bonds involving hydrogen atoms were constrained using the LINCS algorithm (17). Non-bonded van der waals interactions were cut-off at 12 Å and were force switched to zero between 10 and 12 Å. The temperature was maintained throughout the simulation by the Nosé-Hoover thermostat with a time constant of 1 ps. For constant pressure coupling, a semi-isotropic Parrinello-Rahman barostat with a time constant of 5 ps and a compressibility of 4.5×10^{-5} bar was used. Molecular dynamics trajectories were analyzed using VMD 1.9.4. The root-mean-square deviation (RMSD) of backbone atoms was computed after a least-squares fit to the initial structure. Molecular structure images were prepared using PyMOL 2.2.0. Electrostatic potential surfaces were rendered using the APBS Electrostatics Plugin for PyMOL.

Clinical data analysis. Fragments per kilobase million (FPKM) normalized transcriptomic data together with the clinical data were obtained from The Cancer Genome Atlas (TCGA) research network under project ID TCGA-CHOL (18). Plots were generated in R version 3.6.1 (19). Statistical comparisons were performed using Wilcoxon rank-sum test.

SI References

1. Uthaisar K, et al. (2016) Establishment and characterization of a novel human cholangiocarcinoma cell line with high metastatic activity. *Oncol Rep* 36(3):1435–1446.
2. Saentaweesuk W, et al. (2018) Activation of vimentin is critical to promote a metastatic potential of cholangiocarcinoma cells. *Oncol Res* 26(4):605–616.
3. Sripa B, et al. (2020) Functional and genetic characterization of three cell lines derived from an Opisthorchis viverrini-associated cholangiocarcinoma patient. *Hum Cell*. doi:10.1007/s13577-020-00334-w.
4. Hamorsky KT, et al. (2019) Engineering of a Lectibody Targeting High-Mannose-Type Glycans of the HIV Envelope. *Mol Ther*. doi:10.1016/j.ymthe.2019.07.021.
5. Kasinger LES, Dent MW, Mahajan G, Hamorsky KT, Matoba N (2019) A novel anti-HIV-1 bispecific bNAb-lectin fusion protein engineered in a plant-based transient expression system. *Plant Biotechnol J* 17(8):1646–1656.

6. Kronewitter SR, et al. (2009) The development of retrosynthetic glycan libraries to profile and classify the human serum N-linked glycome. *Proteomics* 9(11):2986–2994.
7. Park DD, et al. (2018) Membrane glycomics reveal heterogeneity and quantitative distribution of cell surface sialylation. *Chem Sci* 9(29):6271–6285.
8. Xu G, et al. (2019) Unveiling the metabolic fate of monosaccharides in cell membranes with glycomic and glycoproteomic analyses. *Chem Sci* 10(29):6992–7002.
9. Crooks GE, Hon G, Chandonia JM, Brenner SE (2004) WebLogo: A sequence logo generator. *Genome Res* 14(6):1188–1190.
10. Mi H, Muruganujan A, Ebert D, Huang X, Thomas PD (2019) PANTHER version 14: More genomes, a new PANTHER GO-slim and improvements in enrichment analysis tools. *Nucleic Acids Res* 47(D1):D419–D426.
11. Kirschner KN, et al. (2008) GLYCAM06: A generalizable biomolecular force field. carbohydrates. *J Comput Chem* 29(4):622–655.
12. Hubbard SJ, Thornton JM (1993) NACCESS Computer Program (Department of Biochemistry and Molecular Biology, University College London, London).
13. Jo S, Kim T, Iyer VG, Im W (2008) CHARMM-GUI: A web-based graphical user interface for CHARMM. *J Comput Chem* 29(11):1859–1865.
14. Abraham MJ, et al. (2015) Gromacs: High performance molecular simulations through multi-level parallelism from laptops to supercomputers. *SoftwareX* 1–2:19–25.
15. Towns J, et al. (2014) XSEDE: Accelerating scientific discovery. *Comput Sci Eng* 16:62–74.
16. Huang J, et al. (2017) CHARMM36m: An improved force field for folded and intrinsically disordered proteins. *Nat Methods* 14(1):71–73.
17. Hess B, Bekker H, Berendsen HJC, Fraaije JGEM (1997) LINCS: A Linear Constraint Solver for molecular simulations. *J Comput Chem* 18(12):1463–1472.
18. Weinstein JN, et al. (2013) The cancer genome atlas pan-cancer analysis project. *Nat Genet* 45(10):1113–1120.
19. Villanueva RAM, Chen ZJ (2019) ggplot2: Elegant Graphics for Data Analysis (2nd ed.). *Meas Interdiscip Res Perspect* 17(3):160–167.

Supplementary Figure Legends

Figure S1. Dose-response screening of high-mannose glycan expression of CCA cells with addition of kifunensine. Pie charts show the relative abundances of paucimannose and high-mannose type glycans expressed on the membrane of KKU-213A (top) and KKU-213B (bottom) cells. Increasing concentrations of kifunensine are displayed from left to right. Kif, kifunensine; Man, mannose.

Figure S2. Enhancement of migratory and invasive capabilities exhibited by kifunensine-treated ductal carcinoma HCC1954 cells. (A) Characteristics of HCC1954 cells. (B) Relative abundances of N-glycan types expressed on the cell surface of untreated (control) and kifunensine-treated HCC1954 cells as determined by nanoLC-MS. HM, high-mannose type N-glycans; C, complex type N-glycans; H, hybrid type N-glycans; F, fucosylated; S, sialylated. (C) Enumerated cells that passed through an uncoated (migration) or Matrigel-coated (invasion) microporous polycarbonate membrane. Data are represented as mean ± SEM (n=3); **P*<0.05; ***P*<0.01.

Figure S3. Enhancement of lateral migration exhibited by kifunensine-treated colorectal adenocarcinoma Caco-2 cells. (A) Characteristics of Caco-2 cells. (B) The extent to which a scratch wound was closed by untreated or kifunensine-treated Caco-2 cells over time. (C) Percent closure is presented as a measure that is relative to the distance of the wound at t=0. Data are represented as mean ± SEM (n=3); ***P*<0.01; ****P*<0.001.

Figure S4. Cell aggregation test with increasing concentrations of ConA supplementation. Microscope images of KKU-213AL5 cells after supplementation with ConA at the indicated concentrations. Arrows in the higher magnification images (inset) indicate cell aggregation.

Figure S5. Assessment of metastatic phenotypes of ConA-capped KKU-213AL5 and KKU-213BL5 cells harvested at different cell passages. Representative microscope images of untreated and ConA-capped cells that passed through an uncoated (migration) or Matrigel-coated (invasion) microporous polycarbonate membrane.

Figure S6. Reduction in extended high-mannose glycan abundances in hMAN1A1-KKU-213AL5 compared to PBN-transfected controls.

Figure S7. Frequency plots of amino acid residues ±10 positions from the conserved N-glycosylation consensus sequence, N-X-S/T, of glycopeptides bearing high-mannose type glycans. Residues are indicated as one letter symbols and colored according to their chemical properties. Frequency is proportional to the size of the letter. Plots in the top panels portray the local sequence of identified glycopeptides occupied exclusively with high-mannose type glycans. Plots in the bottom panels portray the local sequence of identified glycopeptides occupied with high-mannose type glycans along with other non-high-mannose type N-glycans.

Figure S8. Characterization of differentially regulated membrane glycoproteins in metastatic CCA. Protein class distribution of (A) all high-mannose-containing glycoproteins identified in KKU-213AL5 and (B) glycoproteins that presented higher abundances of high-mannose glycoforms in KKU-213AL5 in comparison to KKU-213A.

Figure S9. Stick representation of energy minimized Man 5 and Man 9 rotational isomers. Gauche-trans or gauche-gauche conformations about the C6-C7 bond between residues 3 and 4 and between residues 4 and 6 give rise to four stable conformations of Man 5 (top) and of Man 9 (bottom), respectively. Carbon atoms are colored according to structure (Man 5 or Man 9). Hydrogen, oxygen, and nitrogen atoms are colored white, red, and blue, respectively.

Figure S10. Superposition of docked structures and solved (template) structures of membrane glycoproteins that were upregulated in metastatic CCA in complex with their ligands. Interactions include: (A) transferrin receptor protein 1:transferrin receptor protein 1; (B) dimeric transferrin receptor protein 1:serotransferrin; (C) integrin αV:integrin β3; (D) Integrin αVβ3:Arg-Gly-Asp (RGD) peptide; (D) nicastrin:gamma-secretase subunit APH-1A, PEN-2, presenilin-1 (gamma-secretase); (E) gamma-secretase:Notch 1 fragment. The backbone of the docked structures are shown in ribbon form and the solved structures are shown in cartoon form. Structures are colored by chain. The similarity of aligned structures are indicated by TM scores and RMSDs between common residues in the protein backbone.

Figure S11. Backbone RMSDs for Man 5-bearing and Man 9-bearing transferrin receptor protein 1 relative to the initial structure over the course of the MD simulations.

Figure S12. Superposition of the docked structure of dimeric transferrin receptor protein 1 with or without high-mannose glycosylation and the minimized, equilibrated template structure. The backbone of the docked structure is shown in cartoon form and the crystal structure is shown in ribbon form. Glycan structures in the docked solutions are represented as sticks. Glycan structures in the solved structures are represented as lines. Protein structures are colored by chain. The similarity of aligned structures are indicated by TM scores and RMSDs between common residues in the protein backbone.

Figure S1.

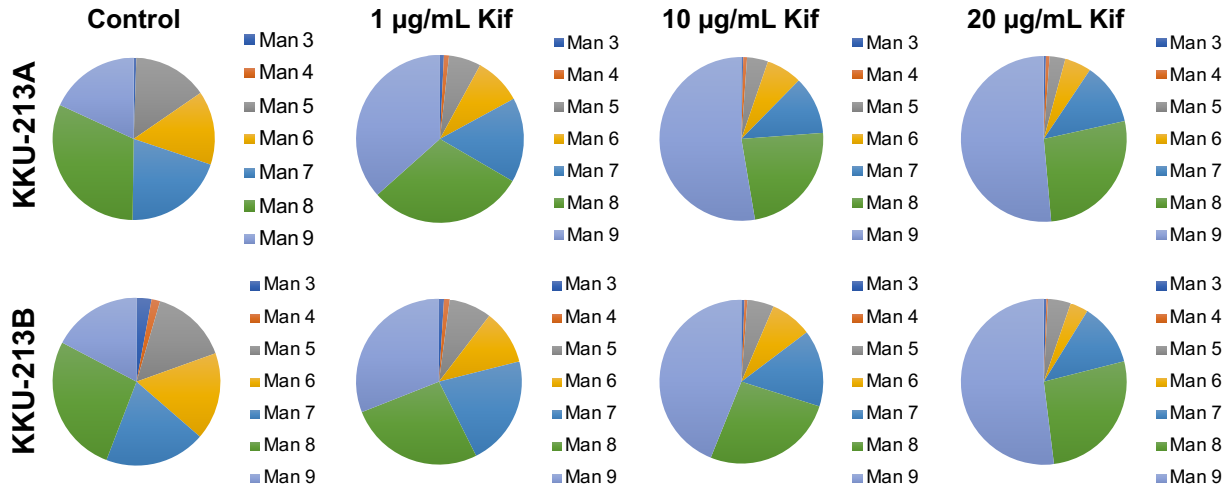
Control
1 µg/mL Kif
10 µg/mL Kif
20 µg/mL Kif
KKU-213A
KKU-213B
Man 3
Man 4
Man 5
Man 6
Man 7
Man 8
Man 9

Figure S2.

A

	Species	Sex	Age	Disease	Tissue	Cell Type
HCC1954	Homo sapiens	Female	61 years	TNM stage IIA, grade 3, ductal carcinoma	mammary gland; breast/duct	Epithelial

B

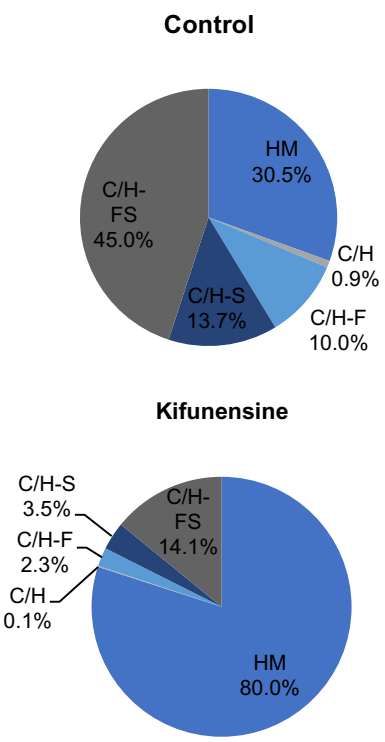

C

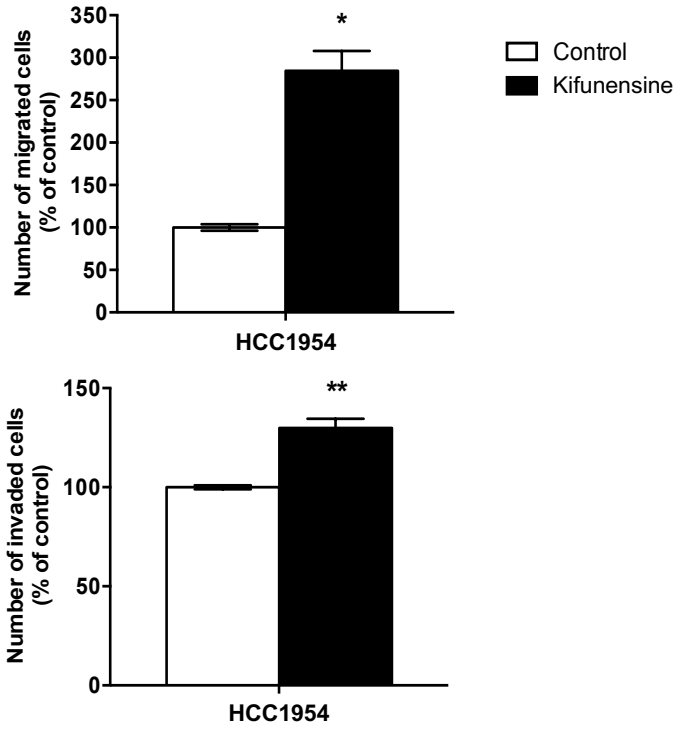

Figure S3.

A

	Species	Sex	Age	Disease	Tissue	Cell Type
Caco-2	Homo sapiens	Male	72 years	Colorectal adenocarcinoma	Colon	Epithelial

B

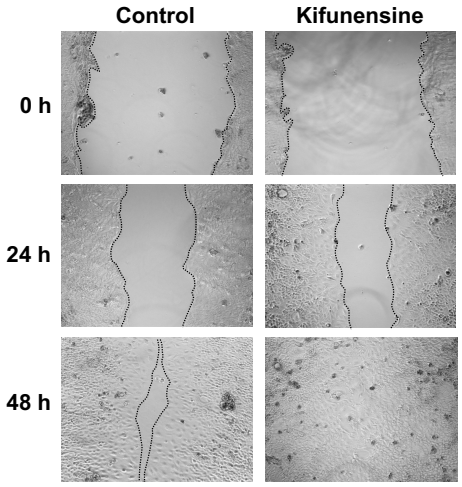

C

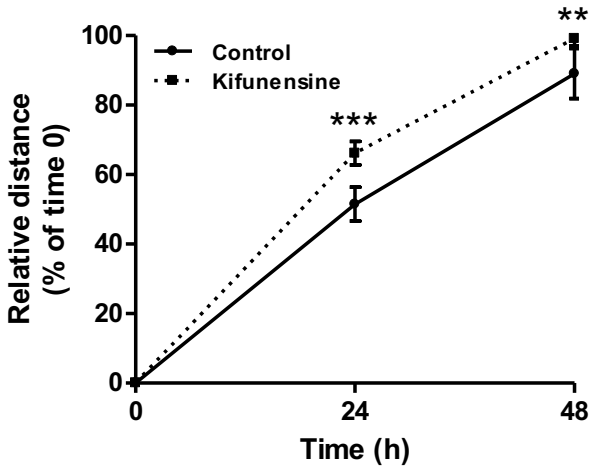

Figure S4.

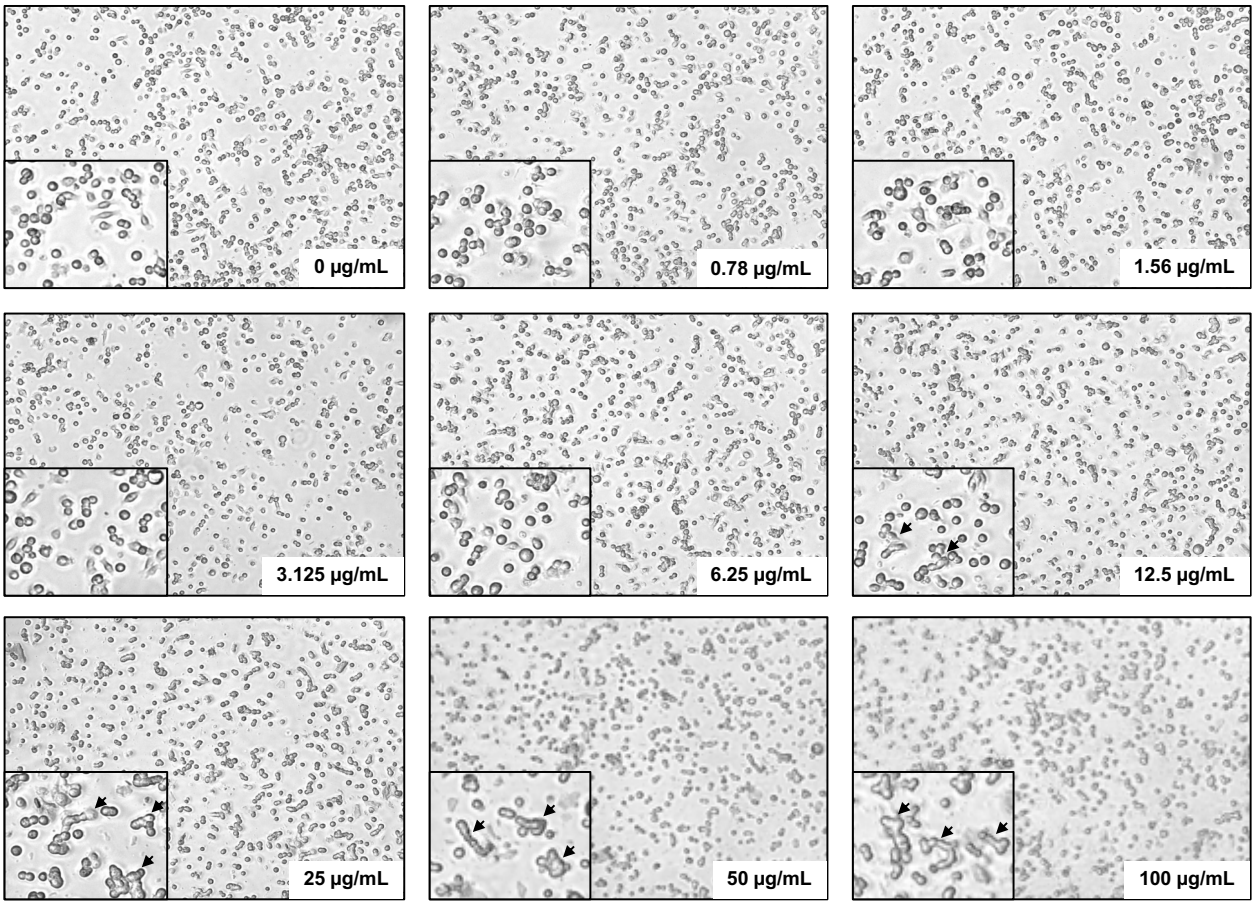
0 μg/mL
0.78 μg/mL
1.56 μg/mL
3.125 μg/mL
6.25 μg/mL
12.5 μg/mL
25 μg/mL
50 μg/mL
100 μg/mL

Figure S5.

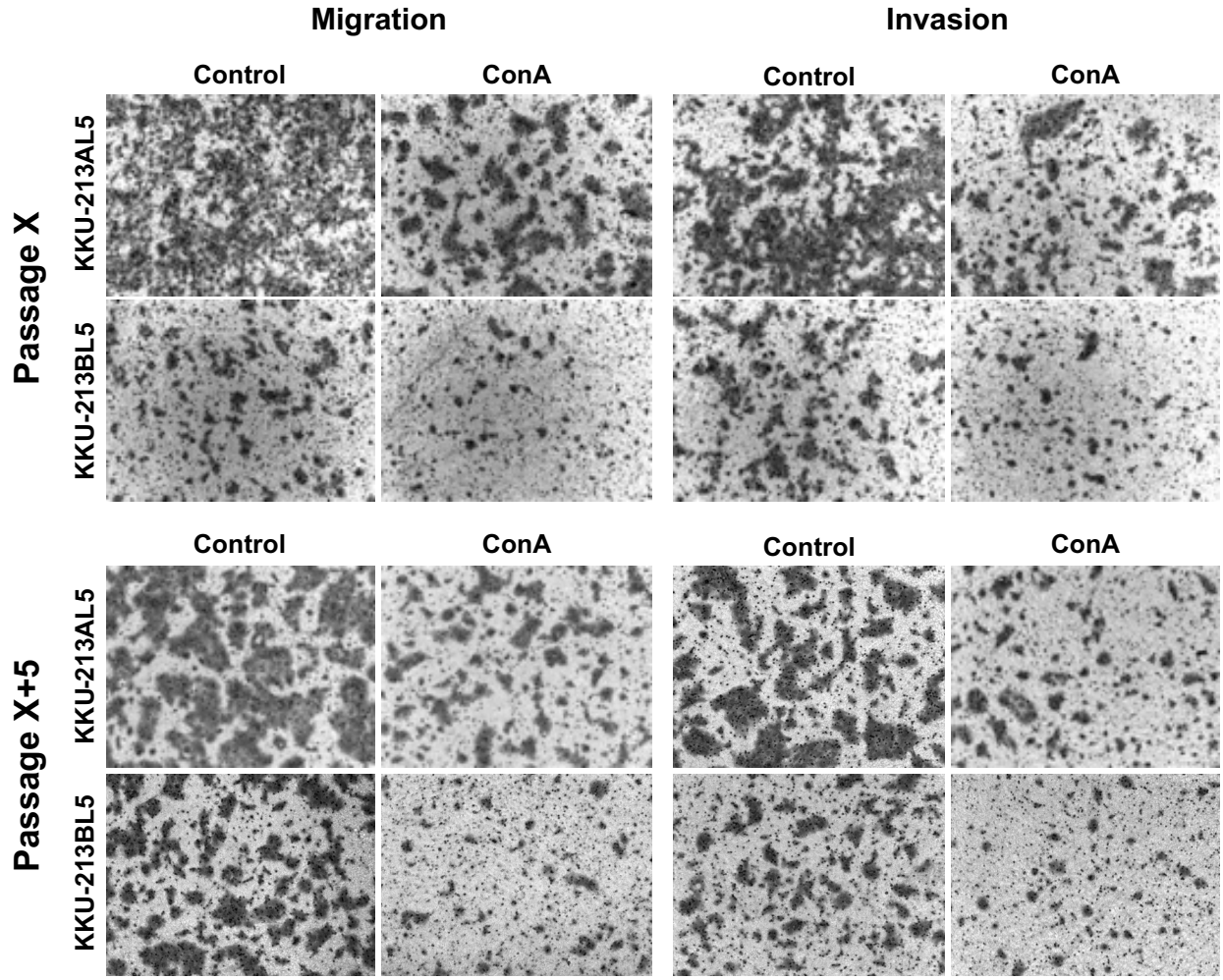
Migration
Invasion
Control
ConA
Control
ConA
Passage X
KKU-213AL5
KKU-213BL5
Control
ConA
Control
ConA
Passage X+5
KKU-213AL5
KKU-213BL5

Figure S6.

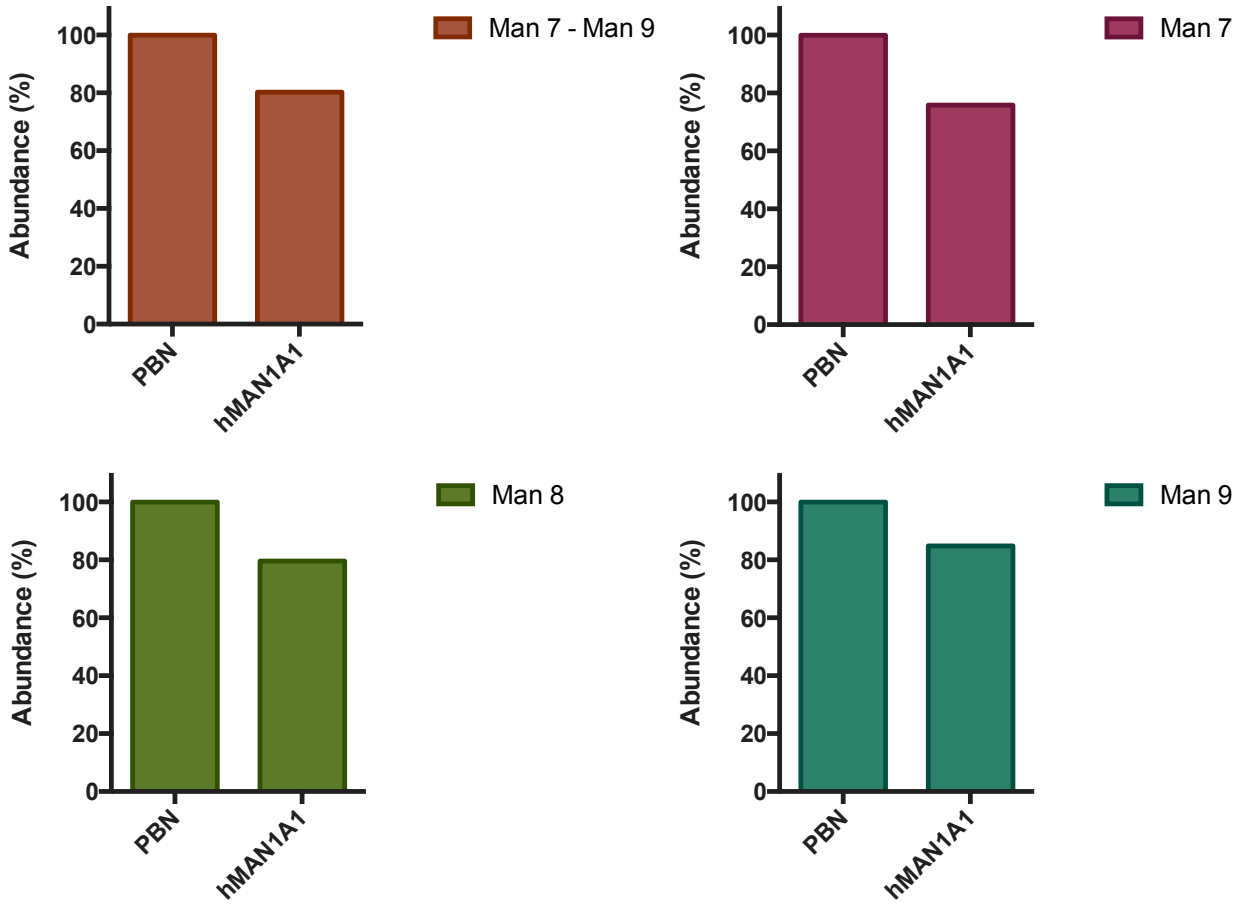
Man 7 - Man 9
Abundance (%)
100
80
60
40
20
0
PBN
hMAN1A1
Man 7
Abundance (%)
100
80
60
40
20
0
PBN
hMAN1A1
Man 8
Abundance (%)
100
80
60
40
20
0
PBN
hMAN1A1
Man 9
Abundance (%)
100
80
60
40
20
0
PBN
hMAN1A1

Figure S7.

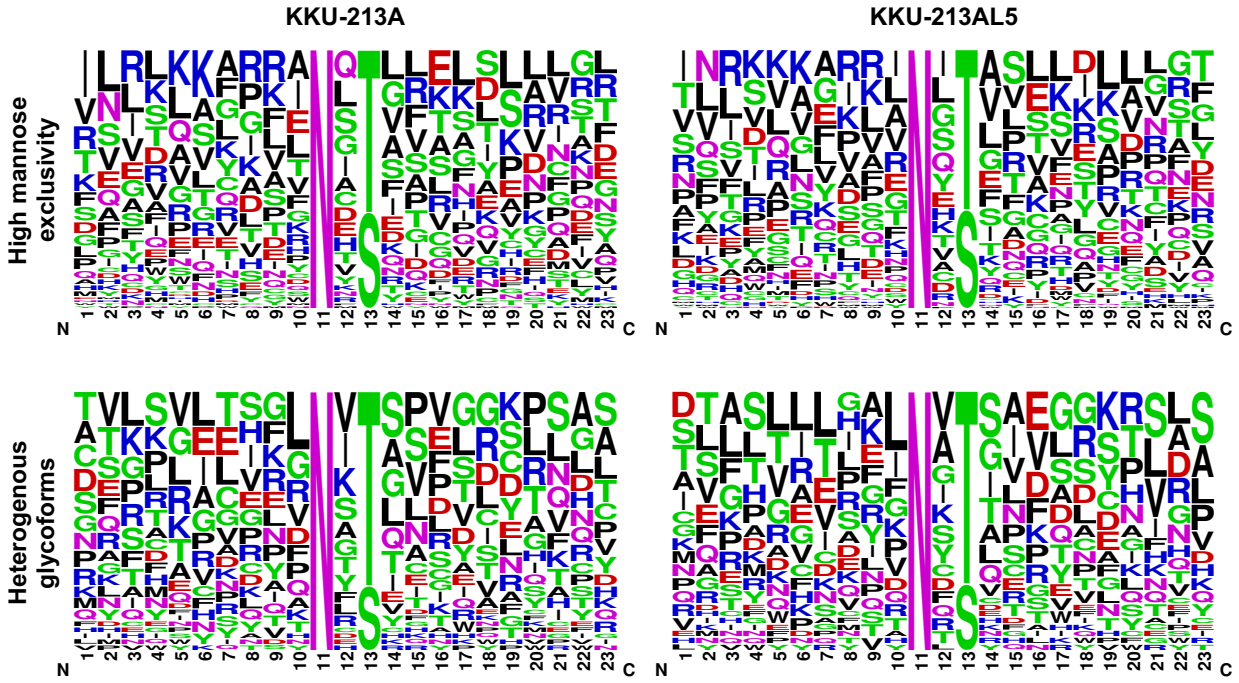
KKU-213A
KKU-213AL5
High mannose exclusivity
Heterogenous glycoforms
N
C

Figure S8.

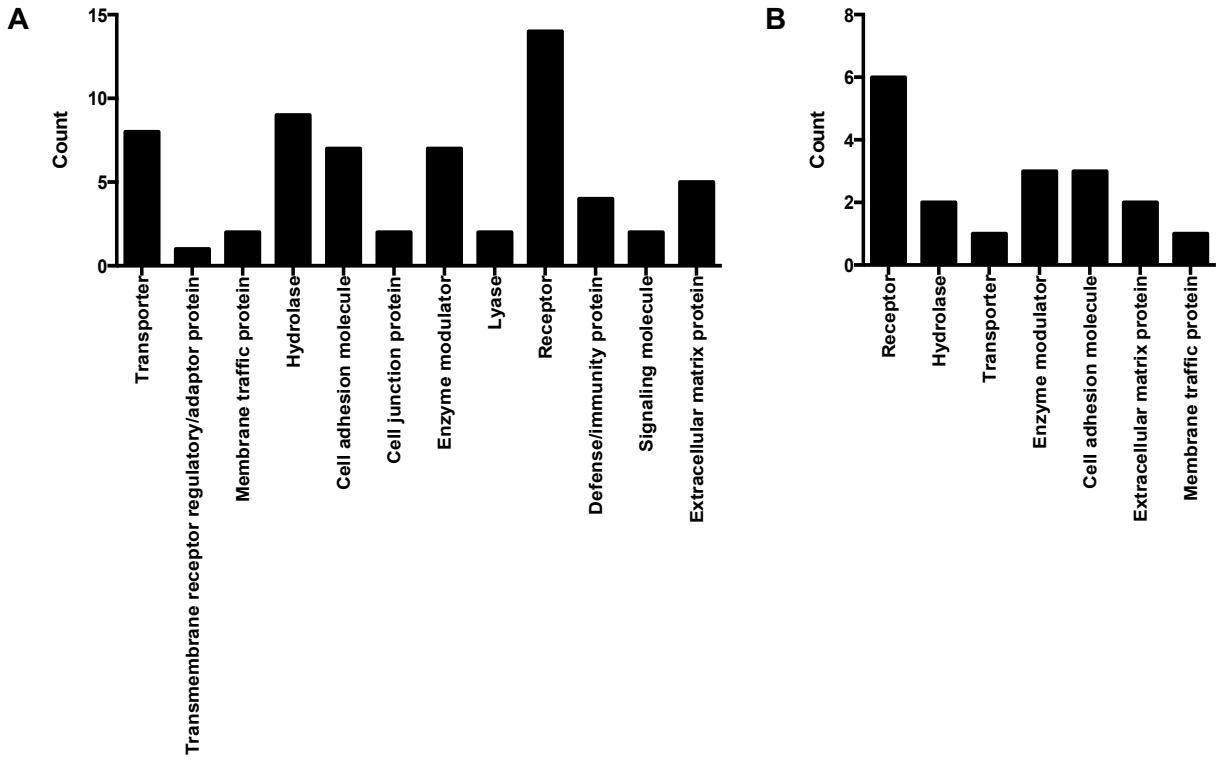
A
Count
15
10
5
0
Transporter
Transmembrane receptor regulatory/adaptor protein
Membrane traffic protein
Hydrolase
Cell adhesion molecule
Cell junction protein
Enzyme modulator
Lyase
Receptor
Defense/immunity protein
Signaling molecule
Extracellular matrix protein
B
Count
8
6
4
2
0
Receptor
Hydrolase
Transporter
Enzyme modulator
Cell adhesion molecule
Extracellular matrix protein
Membrane traffic protein

Figure S9.

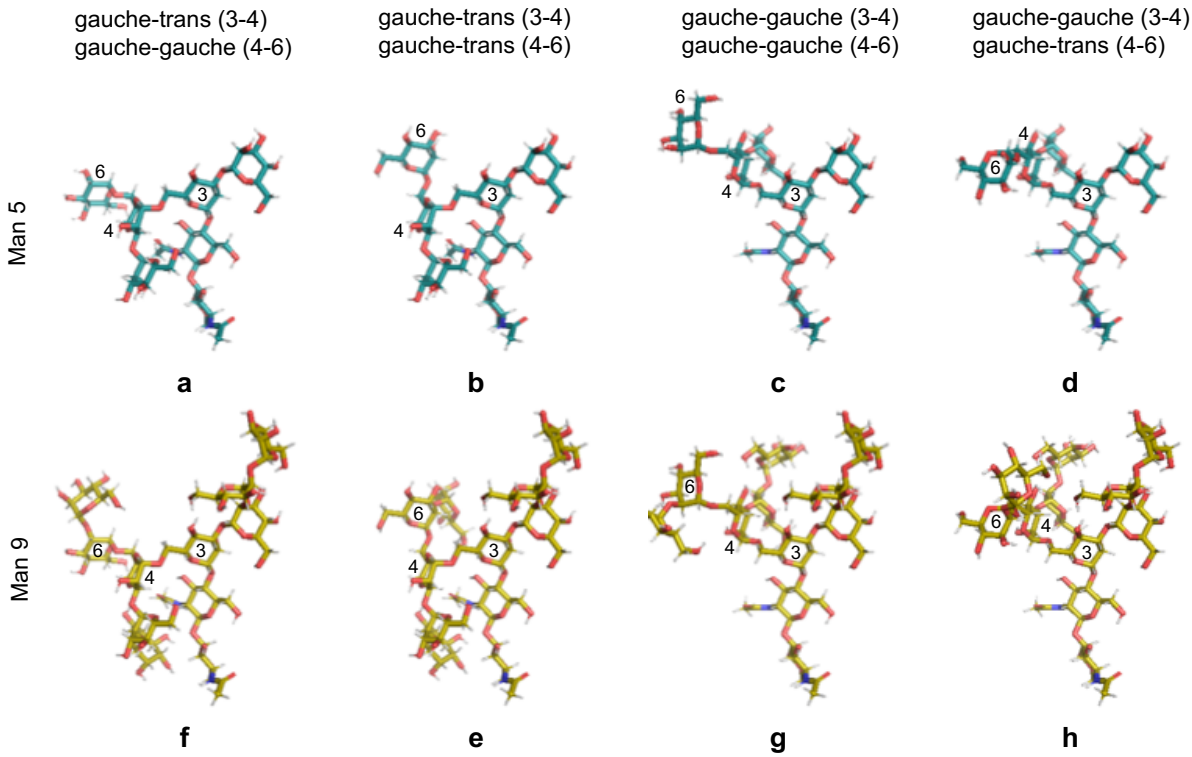
gauche-trans (3-4)
gauche-gauche (4-6)
gauche-trans (3-4)
gauche-trans (4-6)
gauche-gauche (3-4)
gauche-gauche (4-6)
gauche-gauche (3-4)
gauche-trans (4-6)
Man 5
Man 9
a
b
c
d
f
e
g
h

Figure S10.

A

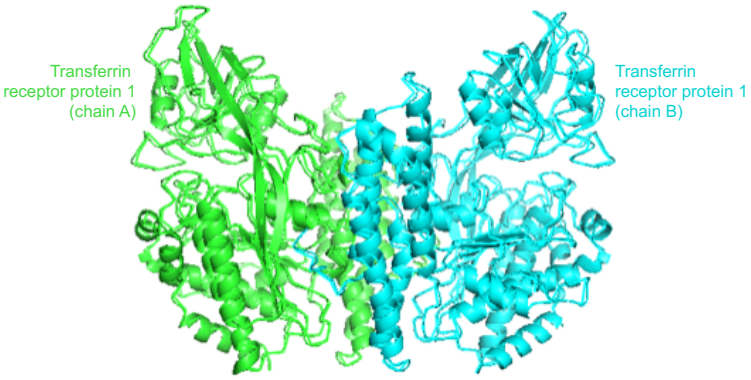

Transferrin receptor protein 1 : transferrin receptor protein 1
TM score = 0.998
RMSD = 0.578 Å (1278 residues)

B

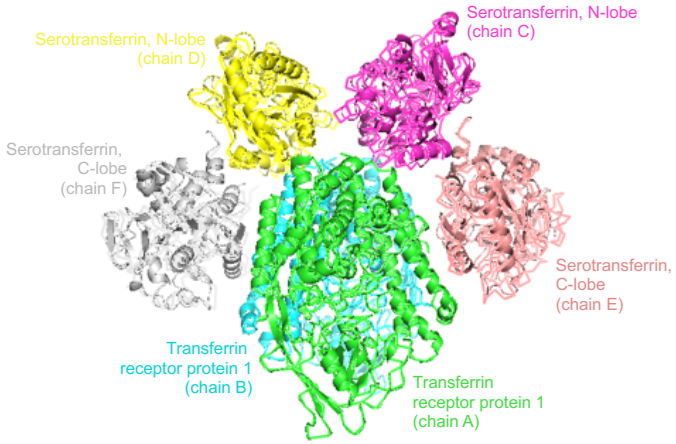

Transferrin receptor protein 1 dimer : serotransferrin (C-, N-lobe)
TM score = 0.999
RMSD = 0.413 Å (20562 residues)

C

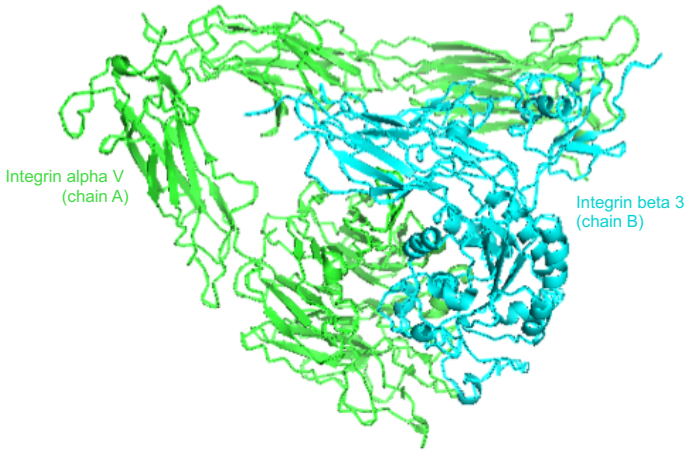

Integrin αV : Integrin β3
TM score = 0.999
RMSD = 0.379 Å (1466 residues)

D

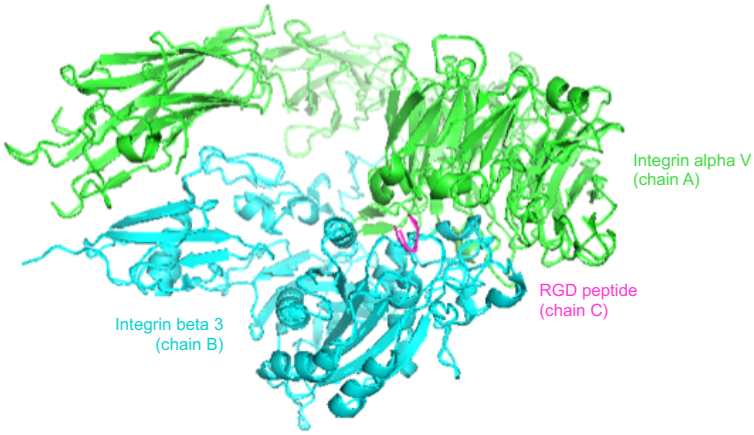

Integrin αVβ3 : RGD peptide
TM score = 1.000
RMSD = 0.047 Å (1470 residues)

E

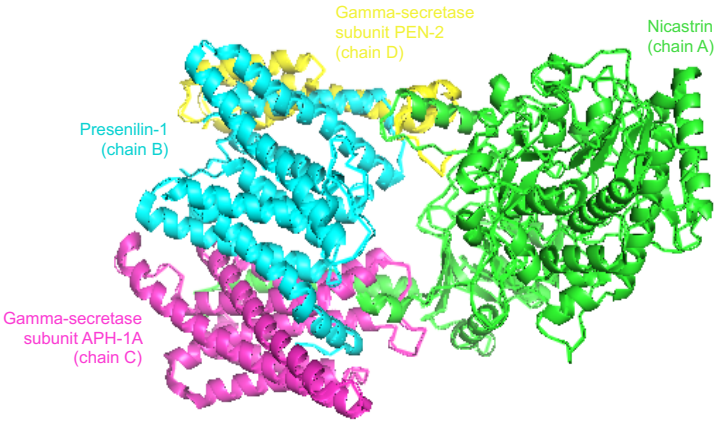

Nicastrin : gamma-secreatase subunit APH-1A, PEN-2, presenilin-1
TM score = 0.998
RMSD = 0.511 Å (1294 residues)

F

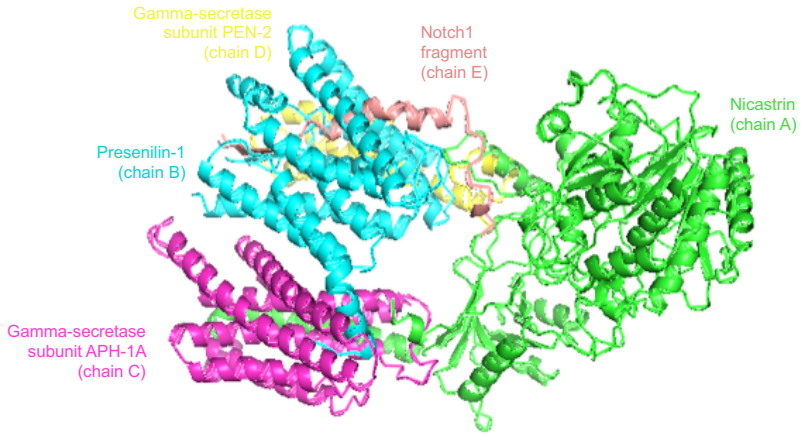

γ-secretase : Notch fragment
TM score = 1.000
RMSD = 0.184 Å (1363 residues)

Figure S11.

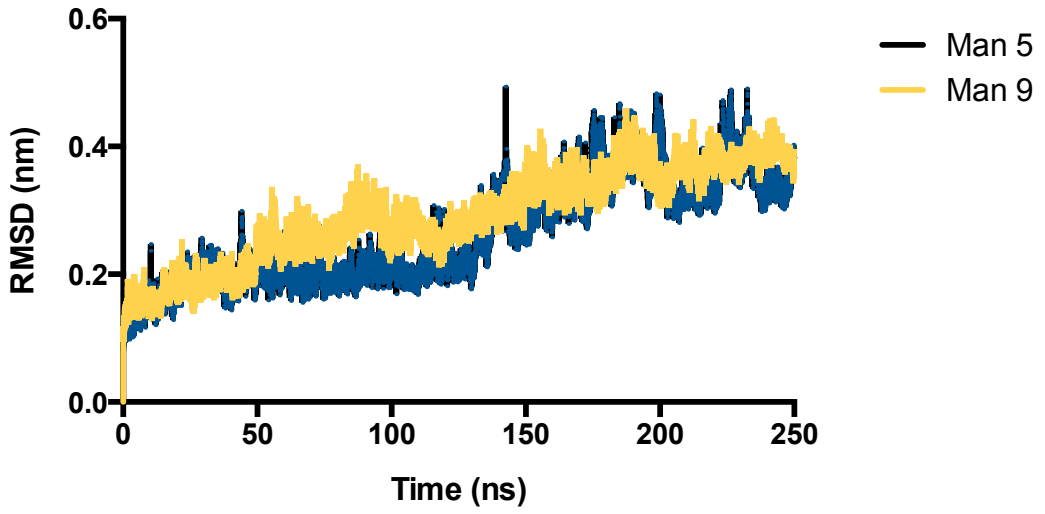

Figure S12.

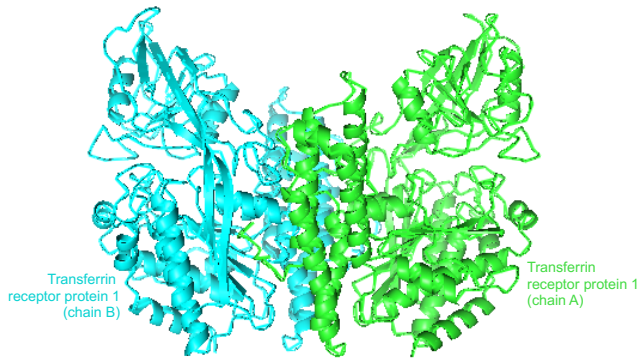

TFRC : TFRC (min, eq)
TM score = 0.999
RMSD = 0.392 Å (1278 residues)

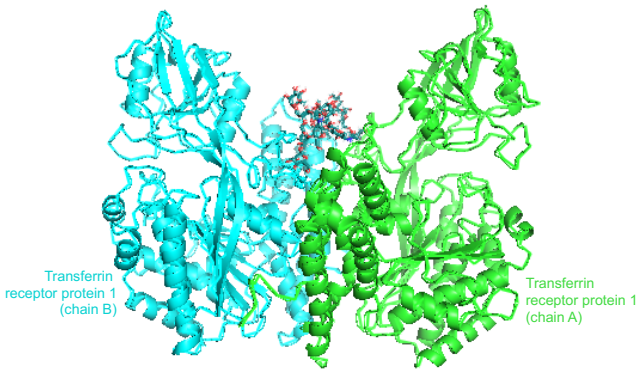

N727-Man 5-TFRC : N727-Man 5-TFRC (production)
TM score = 0.998
RMSD = 0.477 Å (1278 residues)

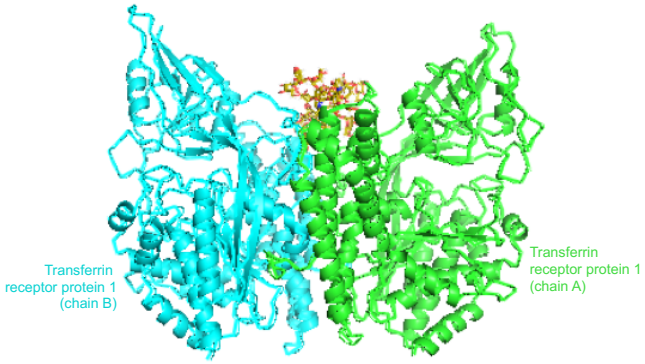

N727-Man 9-TFRC : N727-Man 9-TFRC (production)
TM score = 0.998
RMSD = 0.567 Å (1278 residues)

Supplementary Video Legends

Video S1. Time-lapse video microscopy of parental cholangiocarcinoma KKU-213A cells during the course of a 24 h incubation at 37°C. Frame rate, 20 frames/s; scale bars, 10 μm.

Video S2. Time-lapse video microscopy of metastatic cholangiocarcinoma KKU-213AL5 cells during the course of a 24 h incubation at 37°C. Frame rate, 20 frames/s; scale bars, 10 μm.

Dataset Legends

Dataset S1. Glycosylated membrane proteins of parental cholangiocarcinoma KKU-213A cells occupied with high-mannose type N-glycans.

Dataset S2. High-mannose-bearing membrane peptides of parental cholangiocarcinoma KKU-213A cells. Occupied glycan sites are boldfaced. Other modifications include carbamidomethylation of cysteine residues [+57.021], pyroglutamate conversion of glutamine residues [-17.027], and pyroglutamate conversion of glutamate residues [-18.011].

Dataset S3. Glycosylated membrane proteins of metastatic cholangiocarcinoma KKU-213AL5 cells occupied with high-mannose type N-glycans.

Dataset S4. High-mannose-bearing membrane peptides of metatastic cholangiocarcinoma KKU-213AL5 cells. Occupied glycan sites are boldfaced. Other modifications include carbamidomethylation of cysteine residues [+57.021] and pyroglutamate conversion of glutamine residues [-17.027].